RSC Advances

PAPER

View Article Online
View Journal | View Issue

Cite this: *RSC Adv.*, 2017, **7**, 42940

Enhanced photoelectric performance of (2Al, S) co-doped rutile SnO_2†

Minmin Guo,[a] Huimin Yang,[a] Mengting Gao,[a] Erhui Zhang,[a] Zhenhai Liang *[a] and Peide Han [b]

In this study, theoretical calculations and experiments have been carried out to investigate the photoelectric performance of (2Al, S) co-doped rutile SnO_2. The electronic structures are studied by density functional theory (DFT). It is found that the metal Al can assist the bonding of the incorporated S with the neighboring O in SnO_2, introducing new energy levels in the forbidden band of SnO_2, which enhance the photoelectric performance. Meanwhile, the experiments are conducted to verify this. The (2Al, S) co-doped SnO_2 with different doping ratios are prepared by a hydrothermal method. The samples are characterized by X-ray powder diffraction (XRD), scanning electron microscopy (SEM) and X-ray photoelectron spectroscopy (XPS). Results show that all the samples have rutile structure without any extra phase, and the dopant S^{2-} ion was implanted into the crystalline lattice of (2Al, S) co-doped SnO_2 and Al dopants replaced Sn atoms. The photoelectric performance tests show Al and S co-doping can improve the photoelectric performance, especially with a doping ratio of 5%, when the photocurrent reaches maximum of 3.0 μA cm^{-2} which is almost twice as much as pure SnO_2, and the impedance is the smallest. The experiments results are consistent with our theoretical calculations. These findings are expected to be helpful for the design of highly active tin oxide-based photoelectric materials.

Received 18th July 2017
Accepted 30th August 2017

DOI: 10.1039/c7ra07891a

rsc.li/rsc-advances

Introduction

SnO_2 is a kind of rutile semiconductor oxide with wide band gap of 3.6 eV.[1,2] It has advantages of good optical transmission to visible light, big ultraviolet absorption coefficient, low preparation temperature, stable chemical property and strong acid and alkali resistance at room temperature.[3–6] Therefore, it can been widely used in organic light emitting diodes (OLED), liquid crystal displays (LCD), solar cells, gas sensors and field effect transistors.[7–11] The preparation and performance of SnO_2 materials have attracted wide attention. However, the photoelectric performance of pure SnO_2 is poor. Doping can adjust the change of band gap and promote the separation of photo-induced electrons and holes, which improves the photoelectric performance. Therefore, research mainly focuses on the influence of doping on the photoelectric performance and stability of SnO_2. Huang *et al.*[12] prepared Zn-doped SnO_2 nanorods by a simple hydrothermal method. The results show that photocatalytic activity of the synthesized Zn-doped SnO_2 nanorods is much higher than pure SnO_2 nanorods and bulk SnO_2 powders. Lee *et al.*[13] studied electrocatalytic activities and stabilities of Pt supported on Sb-doped SnO_2 (ATO) for methanol (MOR) and ethanol (EOR) oxidation reactions. The results show that the Pt/ATO exhibited much higher electrochemical stabilities than Pt supported on carbon (Pt/C). Ahmed *et al.*[14] synthesized Al doped SnO_2 thin films by a sol–gel dip coating technique with different ratios of Al on glass and silicon substrates. The results show doping can enhance its photoelectric performance. With regard to SnO_2 doping, there are many researches on single doping. The reports on co-doping is few, co-doping is firstly proposed during the study on semiconductor materials with single polarity and wide band gap.[15] Two or more elements doping can further improve the photoelectric performance of materials by theory.[16]

In our paper, to gain detailed insight into the effect of Al and S dopants on SnO_2 photoelectric performance, we used density function theory to investigate the electronic structures. Based on the theory calculation, we prepared (2Al, S) co-doping SnO_2 photoelectrode. X-ray diffraction (XRD), scanning electron microscopy (SEM). X-ray photoelectron spectra (XPS) were taken to characterize pure SnO_2 and different ratios of co-doping SnO_2. Meanwhile, photoelectric performance of (2Al, S) co-doped rutile SnO_2 are tested. As a result, the exceptionally high photoelectric performance observed for (2Al, S) co-doped SnO_2 is ascribed to metal Al assisting S–O bonding.

[a]*College of Chemistry and Chemical Engineering, Taiyuan University of Technology, Taiyuan 030024, PR China. E-mail: liangzhenh@sina.com; liangzhenhai@tyut.edu.cn*
[b]*College of Materials Science and Engineering, Taiyuan University of Technology, Taiyuan 030024, PR China*

† Electronic supplementary information (ESI) available. See DOI: 10.1039/c7ra07891a

Results and discussion

Lattice parameters

Fig. 1 shows the optimized configurations of pure SnO_2 and (2Al, S) co-doped SnO_2. Compared with pure SnO_2, the positions of Al atoms and S atom move to a certain degree accompanying the distortion of bonds. The distance of co-planar O and adjacent perpendicular O atom in pure SnO_2 is 2.902 Å. However, for the (2Al, S) co-doped SnO_2, the distance of S and O atoms is 1.641 Å, indicating the formation of S–O covalent bond. The definite lattice parameters are listed in Table 1. The lattice parameters are all bigger than that of pure one, this may because the radius of S^{2-} is bigger than that of O^{2-} radius (O^{2-}: 1.22 Å, S^{2-}: 1.70 Å).

Band structure and density of states

The calculated band gap of pure SnO_2 is 1.07 eV, which is same with other theory calculations.[17] However, the experiment value of SnO_2 band gap is 3.6 eV. The difference may be caused by the underestimation of density functional theory to band gap.[18] The defect of density functional theory leads to smaller forbidden band comparing to experiment value. In this paper, the calculated band gaps are used to compare the changes. Hence, the error does not affect the qualitative analysis on calculation results. As shown in Fig. 2, the band gap of (2Al, S) co-doped SnO_2 is 0.92 eV, while the band gap of pure SnO_2 is 1.07 eV. The difference suggests that (2Al, S) co-doping can narrow the band gap. Further analysis shows that the co-doping introduce fully occupied energy levels, which forms new top of valance band. At the same time, the bottom of conduct band move down.

The total density of states (TDOS) and partial density of states (PDOS) of pure and (2Al, S) co-doped SnO_2 shown in Fig. 3 are discussed to explain the formation mechanism of fully occupied energy levels. The valence band of pure SnO_2 is mainly composed of O 2p state mixing with small Sn 3d state, and the conduction band is constituted of O 2p and Sn 5p states. While for (2Al, S) co-doped SnO_2, the fully occupied energy levels of valence band are the hybridization of O 2p and S 3p states, which indicate the formation of S–O bond. Similar S–O bond can be found for TiO_2 doping.[19] The bonding mechanism (Fig. 4) are as follows.

Table 1 The calculated lattice parameters of pure and (2Al, S) co-doped 2 × 2 × 2 SnO_2

	a (Å)	b (Å)	c (Å)
Pure SnO_2	9.475	9.475	6.373
(2Al, S) co-doped SnO_2	10.065	9.761	6.519

Two metal acceptors Al substitute for two Sn atoms of SnO_2 supercell, introducing two holes. Then, one S atom substitute for adjacent O atom, which make two electrons transfer from S atom to metal acceptors Al due to smaller electron negativity of S atom comparing with O atom. At this point, $3p_z$ orbital of S atom is empty, which make the formation of covalent bond with adjacent O atom possible. The hybridization of p_z orbitals of both S atom and O atom can form bonding orbital σ and antibonding orbital σ*, while their p_x and p_y orbitals can form bonding orbital π and antibonding orbital π*. The fully occupied energy levels are the antibonding orbital π*. The band gap is narrowed by the antibonding orbital π* and conductive band bottom. Therefore, the metal acceptors Al can assist S–O bonding by taking two electrons away from S atom.

SEM analysis

Fig. 5 shows SEM images of different ratios of (2Al, S) co-doped SnO_2. The pure SnO_2 is spherical particle and the surface is nonuniform. For (2Al, S) co-doped SnO_2, the particle sizes decrease. Small particle size can short spreading time of charge carrier from the body to the surface and reduce electron–hole recombination rate, which promote the photocatalytic activity. Different levels of reunion appear in all samples. When the doping ratio is 5%, the particles are more dispersed and the granularity is more uniform comparing with others. Hence, the photoelectric performance is the best.

XRD analysis

Fig. 6 show the XRD patterns of different co-doping ratios of SnO_2 crystal. The peaks appeared at $2\theta = 26.506°$, 33.945° and 51.94°, which are the characteristic peaks of rutile SnO_2.[20,21] The corresponding crystal faces are (110), (101) and (211). No characteristic diffraction peaks of other SnO_2 crystal were found,

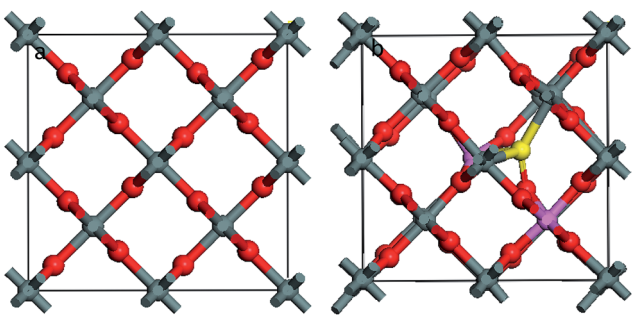

Fig. 1 2 × 2 × 2 SnO_2 supercell (a) and (2Al, S) co-doped SnO_2 supercell (b).

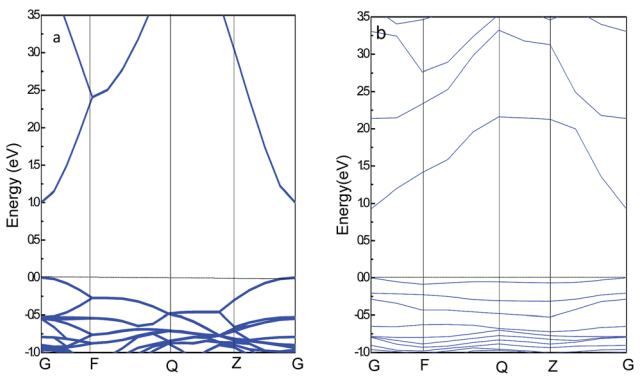

Fig. 2 Band structures of pure SnO_2 (a) and (2Al, S) co-doped SnO_2 (b).

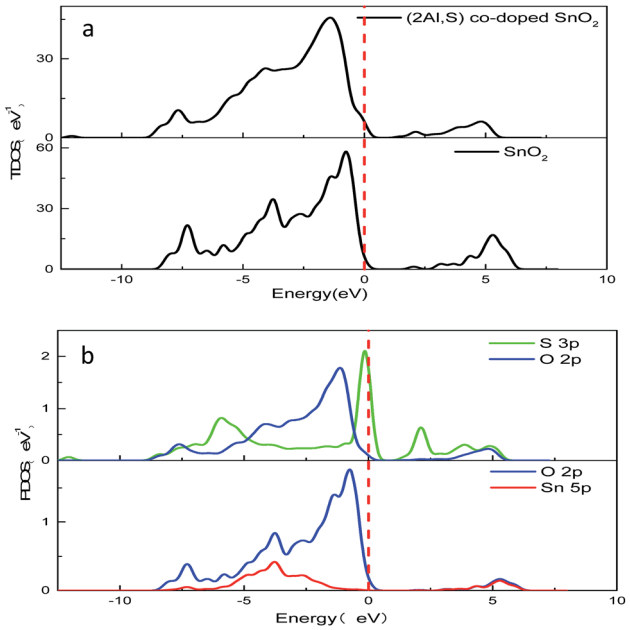

Fig. 3 TDOS (a) and PDOS (b) of pure SnO_2 and (2Al, S) co-doped SnO_2.

indicating that they still keep the structure of rutile SnO_2 after co-doping. In addition, comparing with pure SnO_2, no significant shift in the peak positions was found.

XPS analysis

The XPS spectrum of 5% (2Al, S) co-doping SnO_2 are displayed in Fig. 7. Fig. 7a shows O 1s spectrum, it has two asymmetry peaks, which indicate the presence of two different types of oxygen states.[22] The peaks at 530.88 eV and 531.84 eV belong to lattice oxygen (O^{2-}) and adsorbed oxygen[23,24] respectively. The peak of O 1s at 530.88 eV belongs to SnO_{2-x} structural O atoms or oxygen inside non-stoichiometric oxides within the surface region. The peak at 531.84 eV suggests that oxygen from O_2 molecules of the ambient atmosphere adsorbed on the grains or surface of SnO_2. Compared to O 1s spectrum of pure SnO_2 (Fig. 7e), the peaks move to lower binding energy, which indicates that (2Al, S) co-doped SnO_2 contain more oxygen deficiency. The spectrum of Sn 3d in Fig. 7b have two binding energy peaks. The peaks of Sn $3d_{5/2}$ and Sn $3d_{3/2}$ respectively locate at 486.98 eV and 495.43 eV, suggesting the presence of Sn^{4+}. Also, the different value between Sn $3d_{5/2}$ and Sn $3d_{3/2}$ is 8.45 eV, which is consistent with the standard spectrum of Sn as reported in the Handbook of X-ray photoelectron spectroscopy.[26] However, compared to Sn 3d spectrum of pure SnO_2 (Fig. 7f), the peaks moves towards high binding energy. The generation of chemical displacement is not only the potential energy change caused by valence electron transfer, but also the contribution of lattice field. For (2Al, S) co-doped SnO_2, due to the small difference between the electronegativity of Al and Sn, there is no chemical displacement caused by valence electron transfer. The doped Al dispersed in the lattice, causing SnO_2 lattice defects, which can lead to the change of the lattice field, resulting in the increase of binding energy. S 2p XPS spectrum is shown in Fig. 7c, the peaks at 160.95 eV and 162.81 eV indicate

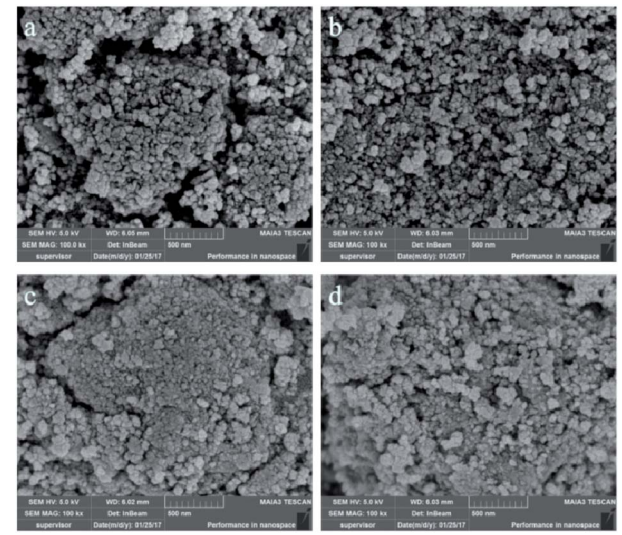

Fig. 5 SEM images of different ratios of (2Al, S) co-doped SnO_2. (a) 0%, (b) 5%, (c) 10% and (d) 15%.

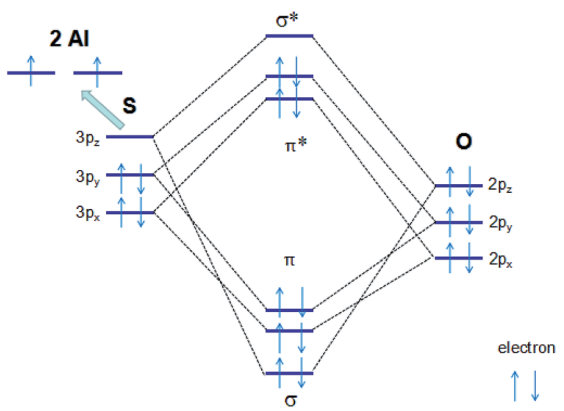

Fig. 4 Schematic plot of bonding mechanism for Al assisted S–O bonding in (2Al, S) co-doped SnO_2.

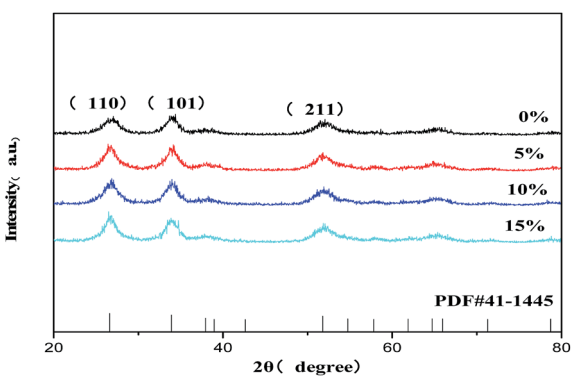

Fig. 6 XRD patterns of pure SnO_2 and different ratios of (2Al, S) co-doped SnO_2.

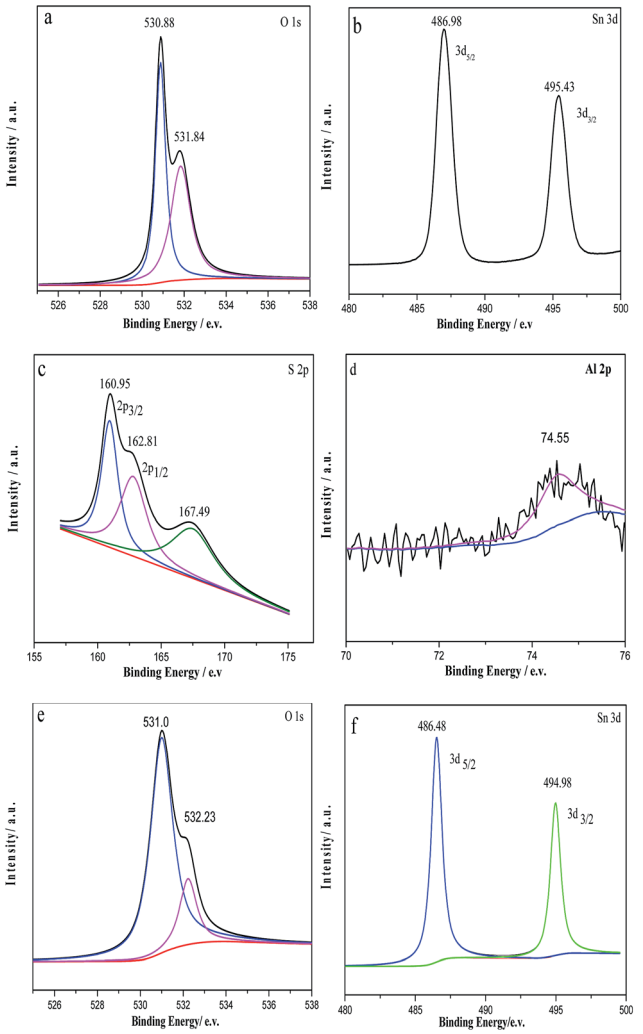

Fig. 7 XPS spectrum of 5% (2Al, S) co-doped SnO_2 (a) O 1s, (b) Sn 3d, (c) S 2p, (d) Al 2p and pure SnO_2 (e) O 1s, (f) Sn 3d.

the presence of S^{2-}. Therefore, we can conclude that S^{2-} ion replace the O^{2-} ion in the lattice of SnO_2. However, it also has a peak at 167.49 eV except the above two peaks, which suggests the existence of S(+6). This may be caused by SO_4^{2-} ions adsorbed on the surface.[25] As shown in Fig. 7d, the binding energy of Al 2p peak at 74.55 eV shows that the Al^{3+} ions replace the Sn^{4+} ions of SnO_2.

Transient photocurrent response test

Fig. 8 display the transient photocurrent response of pure SnO_2 and different doping ratios of (2Al, S) co-doped SnO_2 photoelectrode under 0.5 V bias. The photocurrent value of pure SnO_2, 5%, 10%, and 15% (2Al, S) co-doped SnO_2 reached 1.7, 3.0, 2.4 and 1.2 μA cm^{-2}. When the co-doping amount is 5%, the photocurrent value reaches maximum (the photocurrent values of 0–10% are shown in Fig. S1 and S2†). The common photoelectric metal oxides materials are TiO_2 and ZnO, which show excellent photoelectric properties among metal oxides. Our photocurrent value of 5% (2Al, S) co-doped SnO_2 is almost equal

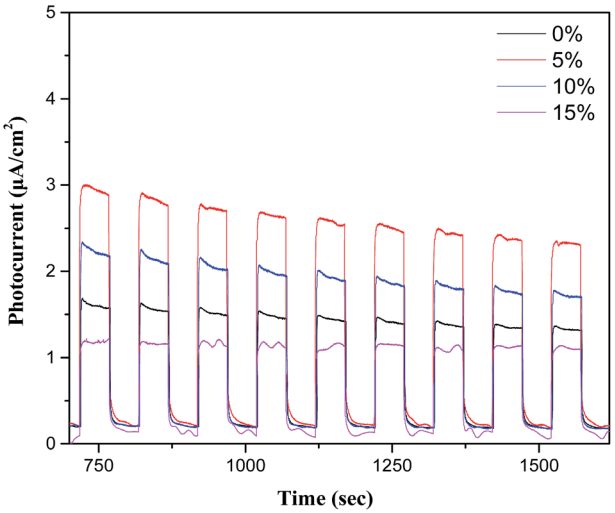

Fig. 8 Transient photocurrent response curve of pure SnO_2 and different ratios of (2Al, S) co-doped SnO_2.

to TiO_2 with etching depth of 387 nm [27] and ZnO under UV light irradiation.[28] As the amount of co-doping continuously increase, the photocurrent value decreases. The results show that suitable amount of co-doping can improve the sunlight utilization rate of SnO_2. 5% (2Al, S) co-doped SnO_2 has small particles and large surface area, which can increase contact area with sunlight. This is consistent with above SEM analysis. Meanwhile, a proper amount of co-doping can inhibit the recombination of photoelectric charge by promoting the separation of photoelectron and hole pairs. In addition, the photocurrent decreases with illumination time, which may due to the slight corrosion of electrodes.

Electrochemical impedance spectroscopy

Electrochemical impedance curve of pure SnO_2 and different doping amount of (2Al, S) co-doped SnO_2 electrodes are shown in Fig. 9. The curve is composed of teratogenic arc of high frequency area and straight line of low-frequency area. The arc

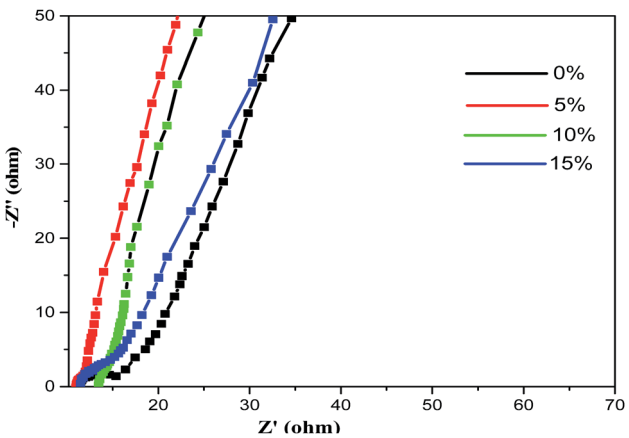

Fig. 9 Electrochemical impedance plots of pure SnO_2 and different ratios of (2Al, S) co-doped SnO_2.

diameter of 5% (2Al, S) co-doped SnO_2 is the smallest, suggesting minimal electrode reaction resistance and more active points of electrochemical reaction. Meanwhile, the slope is relatively higher than others, which shows faster diffusion of ions. In addition, 5% (2Al, S) co-doped SnO_2 has smaller solution resistance, indicating that moderate amount of co-doping can increase the effective contact area of the material and shorten the transmission path of electron and ion.

Conclusions

In summary, DFT calculations have been carried out to detailedly study the effect of photoelectric performance of (2Al, S) co-doped SnO_2. Compared to pure SnO_2, the (2Al, S) co-doped SnO_2 has smaller band gap of 0.92 eV, introducing new energy levels in the forbidden band, which enhance the photoelectric performance in a certain degree. Furthermore, the S–O bonding mechanism assisting by metal Al was explored. The theory calculation can provide evidence supporting experiment conduct. Based on this, different ratios of (2Al, S) co-doped SnO_2 were synthesized by hydrothermal method. In order to study the photoelectric performance, we prepared (2Al, S) co-doped SnO_2 electrodes. The photocurrent of 5% (2Al, S) co-doped SnO_2 reached maximum value of 3.0 μA cm^{-2}. At this point, the impedance is the smallest. These findings can pave the way for developing electrodes with high photoelectric performance in photoelectric catalysis field.

Method

Calculation methods and calculation model

In this study, first-principles calculation was carried out using the Cambridge Serial Total Energy Package (CASTEP) code[29,30] based on density functional theory (DFT).[31] The exchange correlation potential was described with generalised gradient approximation (GGA) in the scheme of Perdew–Burke–Ernzerhof function (PBE).[32,33] The Brillouin zone sampling point K values are $4 \times 4 \times 3$. The cutoff energy for plane waves is set as 340 eV. All geometry structures are fully relaxed until the convergence criteria of energy and force are less than 2.0×10^{-5} eV per atom and 0.03 eV $Å^{-1}$ respectively. The maximum stress is 0.1 GPa.

In calculation, we choose a $2 \times 2 \times 2$ SnO_2 supercell with 48 atoms as calculation model. It has two types of Sn atoms and oxygen atoms respectively. The Sn atoms respectively locate in the vertex and body position. The oxygen atoms can be divided into two classes: one is coplanar with Sn atom, the other is perpendicular to the surface. For (2Al, S) co-doped rutile SnO_2 supercell, two metal Al replace the body-centered Sn atoms, and S atom replace O atom perpendicular to the surface. For an investigation on the electronic structure and ground-state property, the valence electronic configurations are O-$2s^2 2p^4$, S-$3s^2 3p^4$, Sn-$5s^2 5p^2$and Al-$3s^2 3p^1$ states. To obtain reliable results, structural optimization for bulk SnO_2 obtained the following parameters: $a = 4.737$ Å, $c = 3.186$ Å, in good agreement with experiment ($a = 4.734$ Å, $c = 3.187$ Å).[34]

Synthesis of (2Al, S) co-doped SnO_2 electrodes

The synthesis of (2Al, S) co-doped SnO_2 used a one-step hydrothermal method.[35,36] The process is as follows: $SnCl_4 \cdot 5H_2O$ (10.058 g) was firstly dissolved in a beaker with 60 mL deionized water and stirred about 1 h. The sulfourea and $AlCl_3 \cdot 6H_2O$, as S and Al sources, were added into the solution. After stirring for 4 h, the solution was transferred to a 100 mL stainless-steel autoclave with a Teflon liner. The autoclave was sealed and heated at 433 K for 12 h without shaking or stirring during this period. Black precipitate was collected after the autoclave cooled down to room temperature and washed with distilled water several times in order to remove any impurities. After that, the samples were obtained by high temperature calcinations at 573 K for 2 h. Three (2Al, S) co-doped SnO_2 samples with initial doping molar ratios of 5%, 10% and 15% were synthesized. In the preparation, the molar ratio of Al to S is 2 : 1. Pure SnO_2 was synthesized by the same procedure but without any additives.

The above samples were grinded and dispersed in glycerine forming 4 suspensions: 0%, 5%, 10% and 15%. The suspensions were ultrasonicated for 5 min. Then electrodes were prepared by dispensing the suspensions on glass substrates. Finally, the electrodes were burned for 2 h to reserve.

Characterization

The crystal structures of the samples were identified by X-ray diffraction (XRD, X'pert PRO). The morphologies of the samples were characterized by scanning electron microscopy (SEM) with a JSM-7001F (JEOL, Japan). Elemental compositions of the samples were detected by X-ray photoelectron spectroscopy (XPS, Thermo, ESCALAB 250Xi, USA).

Photoelectric performance tests

A trielectrode system was carried out to test the photoelectric performance of SnO_2. The pure SnO_2 and different ratios of (2Al, S) co-doped electrodes, Pt electrode and saturated calomel electrode (SCE) were respectively used as tested electrodes, auxiliary electrode and reference electrode. Na_2SO_4 solution with concentration of 1.0 mol L^{-1} was used as electrolyte solution. The bias voltage is set as 0.5 V.

Conflicts of interest

There are no conflicts to declare.

Acknowledgements

This work is jointly funded by the National Natural Science Foundation of China and Shenhua Group Corp. (Grant No. U1261103), the Natural Science Foundation of Shanxi Province of China. (Grant No. 201601D011023) and Graduate Science and Technology Innovation Fund Project of Shanxi (No. 2017BY053).

References

1 C. Drake and S. Seal, *Appl. Phys. Lett.*, 2007, **90**, 104.

2 S. H. Nam and J. H. Boo, *J. Nanosci. Nanotechnol.*, 2012, **12**, 1559–1562.
3 N. Chiodini, A. Paleari, G. Spinolo and P. Crespi, *J. Non-Cryst. Solids*, 2003, **322**, 266–271.
4 T. R. Giraldi, M. T. Escote, A. P. Maciel, E. Longo and E. R. Leite, *Thin Solid Films*, 2006, **515**, 2678–2685.
5 M. V. Reddy, L. Y. Tse, K. Z. B. Wen and B. V. R. Chowdari, *Mater. Lett.*, 2015, **138**, 231–234.
6 S. Yu, W. Yang, L. Li and W. Zhang, *Sol. Energy Mater. Sol. Cells*, 2016, **144**, 652–656.
7 Y. F. Li, W. J. Yin, R. Deng, R. Chen, J. Chen, Q. Y. Yan, B. Yao, H. D. Sun, S. H. Wei and T. Wu, *NPG Asia Mater.*, 2012, **4**, e30.
8 S. Mihaiu, A. Braileanu, D. Crisan and M. Zaharescu, *Rev. Roum. Chim.*, 2003, **48**, 939–946.
9 A. N. M. Green, E. Palomares, S. A. Haque, J. M. Kroon and J. R. Durrant, *J. Phys. Chem. B*, 2005, **109**, 12525–12533.
10 N. Barsan, M. Schweizer-Berberich and W. Göpel, *Fresenius' J. Anal. Chem.*, 1999, **365**, 287–304.
11 Y. Cheng, R. Yang, J. P. Zheng, Z. L. Wang and P. Xiong, *Mater. Chem. Phys.*, 2012, **137**, 372–380.
12 H. Huang, S. Tian, J. Xu, Z. Xie, D. Zeng, D. Chen and G. Shen, *Nanotechnology*, 2012, **23**, 105502.
13 K. S. Lee, I. S. Park, Y. H. Cho, D. S. Jung, N. Jung, H. Y. Park and Y. E. Sung, *J. Catal.*, 2008, **258**, 143–152.
14 S. F. Ahmed, S. Khan, P. K. Ghosh, M. K. Mitra and K. K. Chattopadhyay, *J. Sol–Gel Sci. Technol.*, 2006, **39**, 241–247.
15 T. Yamamoto and H. Katayama-Yoshida, *Jpn. J. Appl. Phys., Part 2*, 1999, **38**, L166–L169.
16 T. Yamamoto and H. Katayama-Yoshida, *Phys. B*, 2001, **302–303**, 155–162.
17 F. E. H. Hassan, A. Alaeddine, M. Zoaeter and I. Rachidi, *Int. J. Mod. Phys. B*, 2005, **19**, 4081–4092.
18 C. Stampf and C. G. Van de Walle, *Phys. Rev. B*, 1999, **59**, 5521–5535.
19 M. Niu, D. Cheng and D. Cao, *Int. J. Hydrogen Energy*, 2013, **38**, 1251–1257.
20 R. K. Mishra and P. P. Sahay, *Ceram. Int.*, 2012, **38**, 2295–2304.
21 A. K. Singh and U. T. Nakate, *Adv. Nanopart.*, 2013, **02**, 66–70.
22 B. Thomas and B. Skariah, *J. Alloys Compd.*, 2015, **625**, 231–240.
23 P. Y. Liu, J. F. Chen and W. D. Sun, *Vacuum*, 2004, **76**, 7–11.
24 M. Kennedy, Ph.D. Dissertation, University of DuisburgEssen, 2004.
25 T. Ohno, *Appl. Catal., A*, 2004, **265**, 115–121.
26 C. D. Wagner, W. M. Riggs, L. E. Davis and J. F. Moulder, *Handbook of X-Ray Photoelectron Spectroscopy*, Perkin Elmer, Eden Prairie, 1979.
27 S. Y. Luo, B. X. Yan and J. Shen, *ACS Appl. Mater. Interfaces*, 2014, **6**, 8942–8946.
28 Y. J. Wang, R. Shi, J. Lin and Y. F. Zhu, *Energy Environ. Sci.*, 2011, **4**, 2922–2929.
29 B. Andriyevsky, M. Romanyuk and V. Stadnyk, *J. Phys. Chem. Solids*, 2009, **70**, 1109–1112.
30 S. J. Clark, M. D. Segall, C. J. Pickard, P. J. Hasnip, M. J. Probert, K. Refson and M. C. Payne, *Z. Kristallogr.*, 2005, **220**, 567–570.
31 F. M. Bickelhaupt and E. J. Baerends, *Rev. Comput. Chem.*, 2000, **15**, 1–86.
32 E. Fabiano, L. A. Constantin and F. D. Sala, *Int. J. Quantum Chem.*, 2013, **113**, 673–682.
33 J. Nisar, C. Århammar, E. Jämstorp and R. Ahuja, *Phys. Rev. B*, 2011, **84**, 2250–2262.
34 B. Thangaraju, *Thin Solid Films*, 2002, **402**, 71–78.
35 L. M. Fang and X. T. Zu, *Adv. Mater. Res.*, 2007, **26–28**, 683–686.
36 S. Blessi, M. M. L. Sonia, S. Vijayalakshmi and S. Pauline, *Int. J. ChemTech Res.*, 2014, **6**, 2153–2155.